Inorganic Chemistry

ARTICLE

pubs.acs.org/IC

Structural Percolation in the $PbM_{1-x}M_x'O_3$ (M, M′ =Ti, Cr, and V) Perovskites

Ángel M. Arévalo-López*[,†,‡] and Miguel Á. Alario-Franco[†]

[†]Departamento de Química Inorgánica I, Facultad de Ciencias Químicas, Universidad Complutense de Madrid, 28040 Madrid, Spain

Supporting Information

ABSTRACT: Structural properties and the influence of d electrons' insertion in $PbTiO_3$ have been determined in the study of $PbM_{1-x}M_x'O_3$ (M, M′ = Ti, Cr, and V) solid solutions by means of X-ray diffraction, high-resolution transmission electron microscopy, magnetization measurements, and strain mapping analysis. $PbTi_{1-x}V_xO_3$ is the only system that preserves the same space group ($P4mm$) for all x, whereas $PbTi_{1-x}Cr_xO_3$ and $PbV_{1-x}Cr_xO_3$ change to cubic ($Pm\bar{3}m$) at x = 0.30 and 0.4, respectively. These values have been related with the percolation threshold for a cubic net (P_c = 0.31). The microscopy study coincides with the X-ray diffraction determination, and neither supercell nor short-range order maxima are observed. However, for $x \geq 0.7$ in $PbTi_{1-x}Cr_xO_3$ the presence of modulated zones is observed in both the electron diffraction pattern as well as high-resolution transmission electron micrographs, as is typical for $PbCrO_3$.[1] Furthermore, the tetragonal region in $PbV_{1-x}Cr_xO_3$ suffers a great stress because of the contrast of [Cr−O_6] octahedra and [V−O_5] square-based pyramids end members basic units.

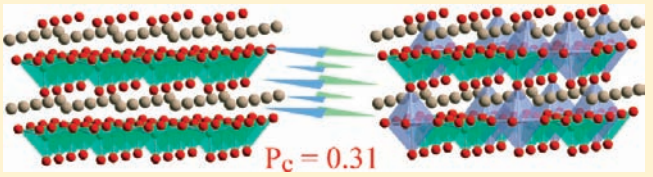

INTRODUCTION

The perovskite $PbTiO_3$ presents a ferroelectric-tetragonal to paraelectric-cubic phase transition with increasing temperature[2] or pressure.[3] Much research has focused on $PbTiO_3$ solid solutions because of their potential applications in piezoelectronic devices, e.g., transducers, actuators, or detectors.[4] Thus, a fundamental understanding of the relationship between the structure and the properties of solid solutions should be investigated. The majority of the substitutions have been done in the B site of the perovskite. The best known solid solutions with simple perovskites are with $BaTiO_3$, $BaZrO_3$, and $PbZrO_3$, where morphotropic phase boundaries (MPB) are present, except in $BaTiO_3$−$BaZrO_3$.[5] MPB in these systems makes reference to a steep boundary that separates two well-defined regions of different symmetry, where the piezoelectric coefficients and dielectric constants exhibit anomalously sharp maxima.[6]

There are also solid solutions with complex perovskites, e.g., $(1-x)Pb(Mg_{1/3}Nb_{2/3})O_3$−$xPbTiO_3$, [PMN]−[PT], or $(1-x)$-$Pb(Zn_{1/3}Nb_{2/3})O_3$−$xPbTiO_3$, [PZN]−[PT], where a transition from normal ferroelectric to relaxor ferroelectric takes place.[7] Understanding the mechanisms that produce the high piezoelectric response of these solid solutions near the MPB has been of interest for more than 50 years.[8−10] Recent studies showed that an intermediate monoclinic phase exists between the rhombohedral and the tetragonal PZT phases,[11] thus answering many of the questions about the nature of the MPB and the underlying basis for the special physical properties around this region.[6] However, Ahart et al. stated that the origin of the MPB is due to the tuning of the high-pressure MPB in pure $PbTiO_3$ to ambient pressure via solid solutions with other lead perovskites.[12]

Following this concept of lowering the MPB to ambient pressure in $PbTiO_3$ and combining it with the insertion of d electrons, we selected two simple lead perovskites, $PbVO_3$ and $PbCrO_3$, and synthesized solid solutions between them.

On the one hand, $PbVO_3$[13] presents the largest tetragonal distortion, c/a = 1.23, among the $PbTiO_3$ compounds and due to the electronic configuration of the V^{4+} ($3d^1$), which promotes the V−O vanadyl bonding with a d_{xy} orbital ordering, also shows a two-dimensional antiferromagnetism with long range order at T_N = 43−50 K.[14] This material has caused a great stir due to its possibility for multiferroicity, finally proved in thin films with an effective piezoelectric coefficient $d_{33} \approx 3.1$ pC/N.[15] However, this behavior has not been observed yet in bulk.

On the other hand, $PbCrO_3$, synthesized under high pressure in the late 1960s,[16] was claimed to be cubic and with antiferromagnetic order at T_N = 160 K.[17,18] However, it has been shown that it presents a compositional modulation which averages to a cubic structure and weak ferromagnetic order with a spin reorientation along ∼100 K.[1,19]

In this article we present the structural, microstructural, and magnetic results of the $PbM_{1-x}M_x'O_3$ (M, M′ = Ti, Cr, and V) solid solutions. Although we could not find a MPB in the sense of an intermediate phase between two well-established regions, we related the structural trends with the percolation limit of a cubic net (P_c = 0.31).

EXPERIMENTAL SECTION

The syntheses were performed in a belt-type apparatus. Corresponding stoichiometric amounts of PbO, TiO_2, VO_2 (99.99% Aldrich pure),

Received: April 2, 2011
Published: June 23, 2011

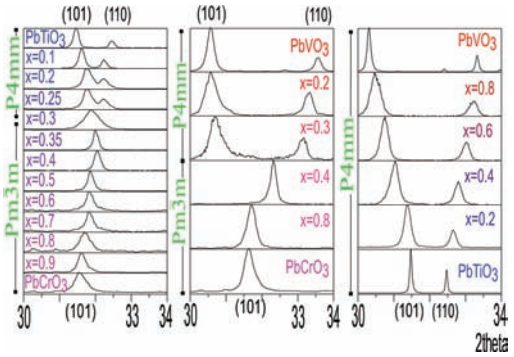

Figure 1. Powder X-ray diffraction data for $PbM_{1-x}M_x'O_3$ (M, M′ = Ti, Cr, and V) solid solutions. They show the evolution of the (101) and (110) peaks as a function of x.

and CrO_2 (BASF) were placed in gold capsules and heated between 800 and 1200 °C under a pressure of 20−80 kbar depending on the x values as detailed in Figure S1 in the Supporting Information.

All of the samples have been characterized by means of X-ray powder diffraction performed in a Panalytical X'Pert PRO MPD (Cu Kα source, Ge monochromator) diffractometer with a step size of 0.033° from 10° to 110° 2θ and a counting time of 10 s/step. The diffraction patterns were analyzed with the Rietveld procedure following the Fullprof program.[20] Backgrounds were fitted using linear interpolation, and peak shapes were modeled by a pseudo-Voigt function. The high- and low-temperature X-ray diffraction experiments were carried out in an X'Pert Pro MPD diffractometer with an Anton Paar HTK1200 high-temperature stage and an Oxford Cryosystems Phenix low-temperature stage, respectively.

High-resolution transmission electron microscopy (HRTEM) and selected area electron diffraction (SAED) were performed on a JEOL JEM 3000F-Field Emission Gun microscope and on a JEOL JEM FX2000, respectively. The composition of each sample was checked by energy-dispersive X-ray spectrometry (EDX; Link Pentafet 5947 model, Oxford Microanalysis Group) by in situ observations. In addition, an ENFINA EELS system placed on the 300 keV microscope for electron energy loss spectra (EELS) acquisition was used. The spectrometer was operated in diffraction mode with a collection semiangle of 8.9 mrad and a dispersion of 0.2 eV/px. Under these conditions, the core-level energy loss spectra are well described by the dipole transition.[21] The background of the spectra has been modeled with an inverse power law, and multiple scattering contributions were removed by a Fourier-ratio deconvolution.[22] We aligned the spectra by fixing the Cr-L_3-edge energy to the value obtained by XPS for Cr^{4+} in CrO_2, 576.3 eV.[23]

Strain mapping analysis was carried out in the high-resolution images following the Peak Pairs method[24] with the help of the Straintool running under Matlab.[25]

Magnetic properties were measured with a Quantum Design MPMS-XL SQUID magnetometer. The temperature dependence of the magnetic susceptibility was measured under an applied magnetic field of 5 kOe in the 2−300 K temperature range.

RESULTS

Crystal Structure. Figure 1 shows the evolution of the powder X-ray diffraction (XRD) patterns for the solid solutions in the range where the (101) and (110) diffraction peaks are present. The complete range of the XRD patterns are shown in Figure S2 in the Supporting Information. The analysis was performed on the basis of the previously determined space groups $Pm\bar{3}m$ and

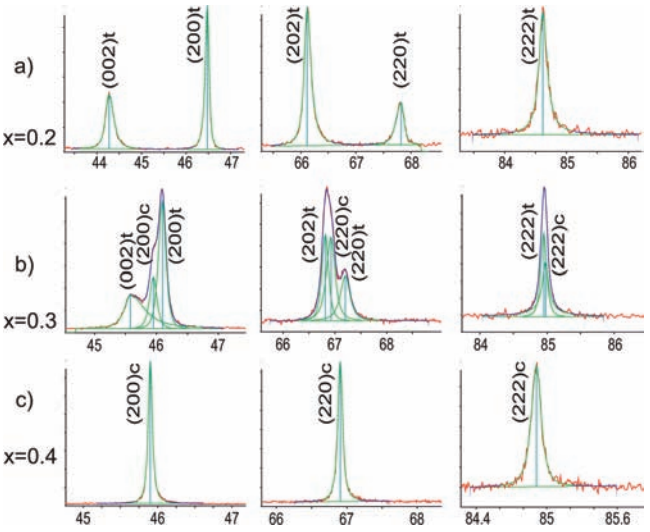

Figure 2. X-ray diffraction profiles for the 002, 022, and 222 reflections of $PbTi_{1-x}Cr_xO_3$ at 300 K for (a) x = 0.2, (b) x = 0.3, and (c) x = 0.4.

$P4mm$ for the cubic and tetragonal phases, respectively.[13,17,26] The $PbTi_{1-x}Cr_xO_3$ solid solution gradually transforms from tetragonal to cubic as the value of x increases, and at x = 0.30 a coexistence of phases is present. On the other hand, the $PbV_{1-x}Cr_xO_3$ solid solution presents an abrupt change from tetragonal to cubic at x > 0.3, and $PbTi_{1-x}V_xO_3$ remains tetragonal for all the different x values.

A reduction in symmetry is a common behavior in solid solutions with Pb in the A site, e.g., $(1-x)Pb(Mg_{1/3}Nb_{2/3})O_3-xPbTiO_3$, $(1-x)Pb(Zn_{1/3}Nb_{2/3})O_3-xPbTiO_3$, and $PbZr_{1-x}Ti_xO_3$.[27−29] For $PbTi_{0.7}Cr_{0.3}O_3$, the split of the (200), (220), and (222) reflections cannot be completely explained by considering only the tetragonal or the cubic system, see Figure 2. Therefore, we followed the analysis developed around the MPB for solid solutions of $PbTiO_3$ and refined the data with the possible space groups: $R3m$ for rhombohedral, Cm or Pm for monoclinic, and $Cmm2$ for orthorhombic symmetry.[27−31] However, the best fit was obtained from a model that considers the coexistence of both tetragonal and cubic phases, see middle of Figure 2. Besides, there was no signature in the SAED experiments suggesting any of these reductions in symmetry (see below). Rietveld refinement along with the fitting statistics for the different models are shown in Figure S3 in the Supporting Information.

In Pb(II) perovskite structures, the lone pair plays a major role. The lone pair occupies approximately the same space as an oxygen ion,[32,33] which causes an especially large distortion when all of the lone pairs are ordered along the same direction and the large tetragonal distortion for both $PbTiO_3$ and $PbVO_3$.[13,34] The structure is also affected by the size of the ionic radii of Cr, Ti, and V, where Cr is significantly smaller than either V or Ti (0.55 < 0.58 < 0.605 Å).[35] Thus, a classical reticular energy model should give a smaller volume per cell unit. The average structure of $PbCrO_3$, however, is larger than expected and cubic. Therefore, the lone pair of Pb(II) in $PbCrO_3$ could be considered in one of two ways: disordered or containing an electronic distribution with no sp character.

For the $PbTi_{1-x}Cr_xO_3$ system, Figure 3 shows that the c cell parameter and the volume V deviate from ideal behavior. This can be understood as follows: introduction of the smaller Cr

dx.doi.org/10.1021/ic200680u |Inorg. Chem. 2011, 50, 7136–7141

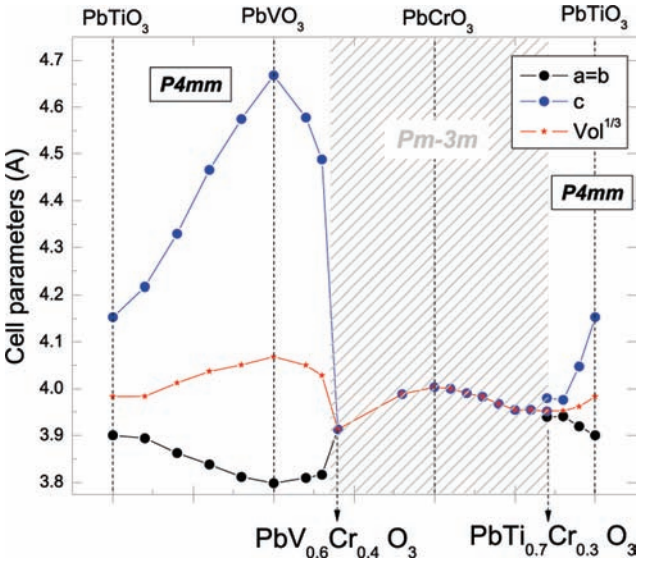

Figure 3. Mole substitution dependence of the cell parameters and the pseudovolume ($(a^2c)^{1/3}$) along the solid solutions $Pb(M_{1-x}M_x')O_3$ (M, M′ = Ti, V, and Cr).

cation causes a decrease in both c and V while the symmetry remains tetragonal, indicating that most of Pb(II)'s lone pairs are oriented along the c axis. However, for $x > 0.3$, the lone pairs start to become more disordered and the phases become cubic, just like $PbCrO_3$. The disorder of the lone pairs results only in small increases of c and V. Finally, with $x > 0.5$, the effect of the lone pairs disorder predominates and c and V increase with x. Thus, the progressive insertion of chromium, where d electrons cause the cation to be located at the center of the octahedron,[36] dominates the behavior at high concentrations and precludes the alignment of the lone pairs.[37]

The deviation from ideal behavior is even stronger for $PbV_{1-x}Cr_xO_3$. After inserting 30% chromium into the $PbVO_3$ lattice, the symmetry changes as well. Finally, in the $PbTi_{1-x}V_xO_3$ solid solution, the trend in the structural parameters also changes with ∼30% of insertion of vanadium. Crystallographic data are summarized in Table 1 in the Supporting Information.

Since $PbTiO_3$ presents a ferroelectric transition at $T_c = 763$ K,[38] we study the evolution of T_c with the change in composition in the tetragonal phases (where T_c is the temperature at which the transition from tetragonal to cubic is complete, i.e., no detectable intensity variation in the $(110)_c$ maximum is observed). Figure 4 shows the evolution with temperature of the $(110)_t$ and $(101)_t$ peaks in the tetragonal phases of $PbTi_{1-x}Cr_xO_3$ system. T_c decreases from 763, to 716, to 630, to 484 K for $x = 0$, 0.1, 0.2, and 0.3 respectively. An extrapolation of the boundary between the cubic and the tetragonal symmetries to higher x suggests that a transition may be present below room temperature (see Figure S4 in the Supporting Information). However, low-temperature XRD for $x = 0.3$, 0.4, and 0.5 at 100 and 150 K indicate that no further transitions are present. This shows that the change in symmetry is very sharp, pointing toward the existence of an MPB.[39] In $PbTi_{1-x}V_xO_3$, $x = 0.2$ transforms to cubic at $T_c = 730$ K (see Figure S5 in the Supporting Information), which is below the T_c of $PbTiO_3$. However, considering the cubic transition of $PbVO_3$, which only occurs at 673 K under 2 GPa (without the use of pressure the compound is decomposed),[40] it follows the trend of increasing c/a with decreasing T_c.

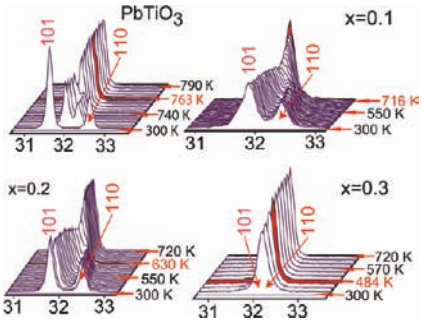

Figure 4. High-temperature X-ray diffraction diagrams for $PbTi_{1-x}Cr_xO_3$ with $x = 0$, 0.1, 0.2, and 0.3 around the (101) and (110) reflections.

For higher V concentrations the samples decompose to $Pb_3V_{2-x}Ti_xO_8$ and/or $Pb_2V_{2-x}Ti_xO_7$ when heated.

Microstructure. We performed a microstructural study of the compounds. The composition of each sample has been analyzed by in situ EDX measurements. The samples have the desired composition within experimental error. $PbCrO_3$ presents lead and oxygen deficiencies as previously published.[1] In order to validate the cation valences on the samples, we realized an EELS study. However, an intrinsic difficulty appears in analyzing these compounds since the V-$L_{2,3}$ edges are localized just before the O−K edges, implying that Pearson's method cannot be applied.[41] Still, with the certainty of the 4+ oxidation state on the B site for $PbTiO_3$[42] and $PbVO_3$[13] combined with the trends observed in the EELS and in the magnetic measurements (see below), we can, therefore, assume the 4+ oxidation state for the B site in the solid solutions; see Figure S7 and discussion in the Supporting Information.

The electron diffraction for the $PbTi_{1-x}Cr_xO_3$ system shows a normal evolution, meaning that neither superstructure nor microdomains appear in the sample, until $x \leq 0.6$. However, due to the split of peaks observed in the XRD pattern for $x = 0.30$, which could indicate a symmetry reduction, the sample was carefully inspected. Nevertheless, electron diffraction was consistent with the XRD data, and no symmetry reduction was detected. For $x > 0.6$, the influence of the $PbCrO_3$-modulated superstructure becomes present and certain regions show its distinctive image. One way to account for the influence at local scale is to apply a strain mapping analysis (SMA, strain being defined as $\varepsilon = (l - l_0)/l_0$ with l_0 being the unstrained length),[24] which measures the local displacements due to some force, in this case provoked by cationic substitution. The HRTEM micrograph for the $PbTi_{0.3}Cr_{0.7}O_3$ sample is presented in Figure 5; coexistence of a cubic (a) and a modulated (b) domain can be observed. Fast Fourier transforms (FFT) of the highlighted zones in the images gave the corresponding maxima to the cubic perovskite and a modulated superstructure. The intensity profiles results in a $17a_p$ periodicity for the modulated superstructure, with a_p being the cubic cell parameter, Figure 5a and 5b, respectively. The SMA clearly shows the tension on the modulated domain when compared with the cubic area. EDX analysis was performed in both regions without any detectable composition difference. This coexistence tendency increases even more for $x = 0.8$ and 0.9, ending in the $PbCrO_3$-modulated structure.

$PbTi_{1-x}V_xO_3$ system evolves as a typical solid solution, as seen by X-ray diffraction. The symmetry is maintained for all of the compositional ranges, and the crystals are strain free. Figure 6a shows the images along [110] and [001] for $PbTi_{0.8}V_{0.2}O_3$ as

dx.doi.org/10.1021/ic200680u |Inorg. Chem. 2011, 50, 7136–7141

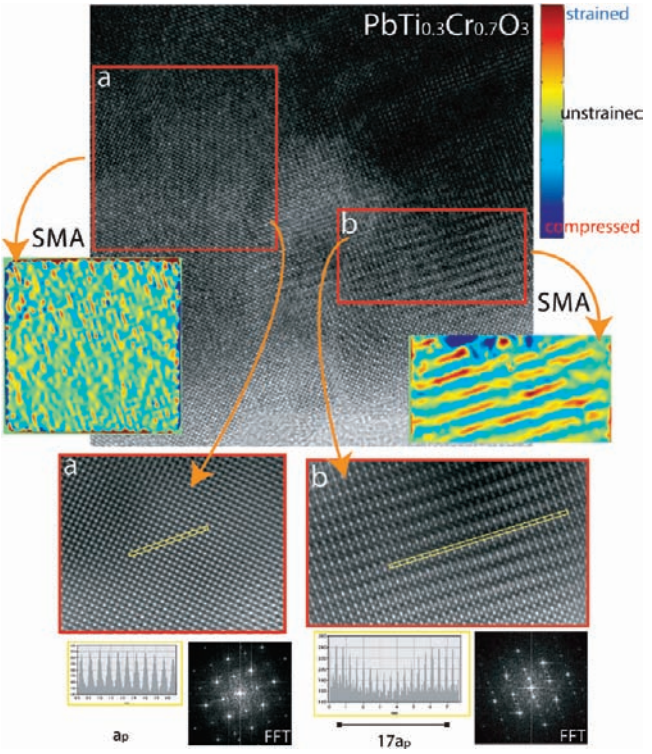

Figure 5. High-resolution micrograph along $[001]_p$ of $PbTi_{0.3}Cr_{0.7}O_3$. Zones with a simple cubic structure (a) and with a modulated structure similar to $PbCrO_3$ with a $17a_p$ period (b) are observed.

representative of the system; the insets show the FFT of the images where no extra peaks can be detected. The simulation of the images coincides with the experiment. However, for the $PbV_{1-x}Cr_xO_3$ system, the scheme changes and highly strained regions are observed for $x \leq 0.3$, Figure 6b. The different coordination preferences of Cr and V cause this great strain in the structure. Chromium is set in the center of the octahedron because of its d electrons,[36] whereas vanadium is placed in a square-based pyramid because of its ordering of the d_{xy} orbitals.[13,14]

Magnetism. Figure 7 shows the magnetic susceptibility temperature dependence for the $PbTi_{1-x}Cr_xO_3$ solid solution. $PbTiO_3$ presents diamagnetic behavior (Ti^{4+} is a d^0 cation). For $x \leq 0.7$, a gradual increase in the magnetic susceptibility is observed, which is due to insertion of chromium. For $x \geq 0.8$, however, the susceptibility decreases, showing behavior more like that of $PbCrO_3$.[19]

The compounds with vanadium present a different problem. First, $PbVO_3$ behaves as a two-dimensional antiferromagnet at $T_N \approx 43-50$ K, which is only observed in single crystals.[14,43] Second, PbV_6O_{11} is a ferromagnetic material at ~90 K.[44] Unfortunately, PbV_6O_{11} is present as a secondary phase in our solid solutions (see Figure S2 in the Supporting Information), and its signal dominates the measurement, making it impossible to study the magnetism in this system. The magnetic susceptibilities for $PbVO_3$, $PbV_{0.8}Ti_{0.2}O_3$, $PbV_{0.9}Cr_{0.1}O_3$, and $PbV_{0.8}Cr_{0.2}O_3$ are shown in Figure S6 in the Supporting Information, where a variation in the ordering temperature can be observed, analogous to the $PbV_{6-x}Fe_xO_{11}$ system, where insertion of iron changes the ordering temperature.[45] This implies that $PbV_{6-x}Ti_xO_{11}$ and $PbV_{6-x}Cr_xO_{11}$ solid solutions also exist and present interesting magnetic properties. This goes, however, beyond the purposes of this work.

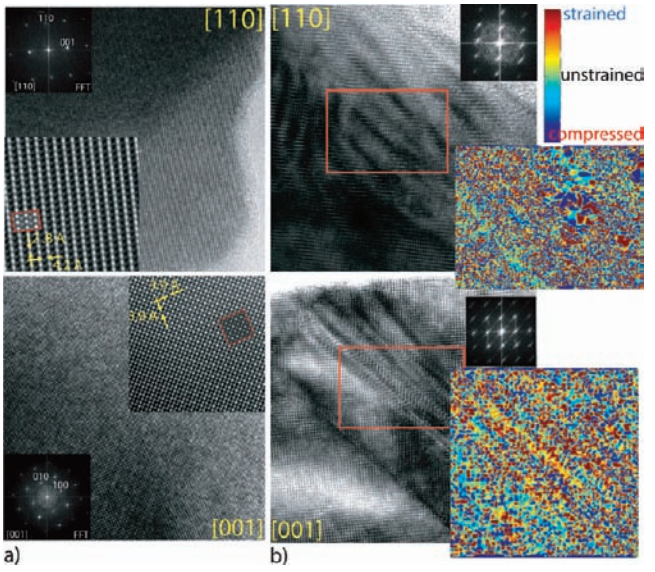

Figure 6. High-resolution images for (a) $PbTi_{0.8}V_{0.2}O_3$ and (b) $PbV_{1-x}Cr_xO_3$ with $x \leq 0.3$. The tension present in the samples is highlighted by strain mapping analysis.

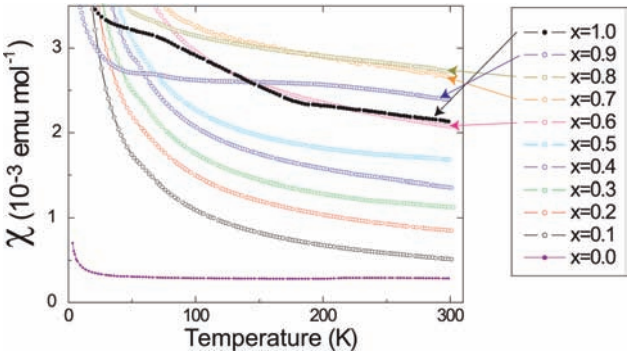

Figure 7. Zero-field-cooled magnetization data for the $PbTi_{1-x}Cr_xO_3$ system.

Discussion and Conclusions. The most striking feature in the B-site content-dependent cell parameter diagram for the $PbM_{1-x}M_x'O_3$ solid solutions, shown in Figure 3, is the change from tetragonal to cubic in two of the three systems. The abrupt changes that occur upon 30% cation insertion signify that the cations' influence on the system is modified at this point. The transition temperature for $PbTi_{0.8}V_{0.2}O_3$ is $T_c = 730$ K (see Figure S5 in the Supporting Information), whereas for higher vanadium concentrations no transition is observed and the samples decompose on heating. Also, for the samples with $x \geq 0.4$, the *a* cell parameter decreases while the *c* parameter increases significantly (Figure 3). Thus, the behavior of the $PbTi_{1-x}V_xO_3$ system is dominated by the ease with which one vanadium V−O bond can break or, in other words, when the vanadyl bond (d_{xy} orbital ordering) becomes active, starting with octahedral coordination for lower concentrations and ending in a square-based pyramid coordination for the higher ones, just as in $PbVO_3$.[13]

In the $PbTi_{1-x}Cr_xO_3$ system, the tetragonal phases, $0 \leq x \leq 0.3$, show a lower T_c as x increases. However, for $x > 0.3$, it is the chromium's proclivity to avoid the off-center shifts, due to the

dx.doi.org/10.1021/ic200680u |*Inorg. Chem.* 2011, 50, 7136–7141

d electrons,[36] that suppresses the transition at high temperature and turns the system into a cubic phase at ambient conditions.

In the case of $PbV_{1-x}Cr_xO_3$, an abrupt transition can also be seen from tetragonal to cubic at $x = 0.4$. This is also explained by the coordination preferences of chromium as in the case of $PbTi_{1-x}Cr_xO_3$.

From the microscopy study we observe the coexistence of cubic and modulated regions in $PbTi_{1-x}Cr_xO_3$ for $x \geq 0.7$, Figure 5. For the samples with $x < 0.7$, there was no signature of modulated domains. This implies that for titanium concentrations higher than ~30% the modulated structure of $PbCrO_3$ is no longer pseudostable. $PbV_{1-x}Cr_xO_3$ shows highly strained regions for $x \leq 0.3$, Figure 6b. This supports the idea of competition between the different structural basic units, the $[Cr-O_6]$ regular octahedron versus the $[V-O_5]$ square-based pyramid. It is also remarkable that for $x > 0.3$ those strained regions are no longer present. The common feature of all three solid solutions is the appearance/disappearance of microstructure/strain at a $x \approx 0.3$ doping concentration.

Both structural and microstructural behaviors can be understood if we consider the percolation threshold for a cubic net $P_c = 0.31$.[46,47] The percolation threshold describes the point at which a dopant in a crystal can be linked in a continuous path in all three directions. For example, if chromium is the dopant in the B site of a perovskite, when $x = 0.31$, each $[Cr-O_6]$ regular octahedron will be linked to at least one other $[Cr-O_6]$ regular octahedron. Thus, the structural transitions in $PbTi_{1-x}V_xO_3$, $PbTi_{1-x}Cr_xO_3$, and $PbV_{1-x}Cr_xO_3$ at about $x = 0.3$ can be explained by a structural percolation of the vanadium in the first case and chromium in the last two. Since $PbV_{1-x}Cr_xO_3$ is percolated by chromium and $PbTi_{1-x}V_xO_3$ by vanadium, we can inspect the role of d electrons in these systems. Examining the data more closely, $PbV_{1-x}Cr_xO_3$'s behavior is dominated by Cr while $PbTi_{1-x}V_xO_3$'s behavior is dominated by V, signifying that each system mimics the behavior of the cation with more d electrons. Thus, introduction of d^2 electrons with chromium destabilizes the d_{xy} orbital ordering present in $PbVO_3$.[14] When the percolation occurs, the square-based pyramids $[V-O_5]$ are no longer favorable; they "*collapse*" to a regular octahedron disordering the lone pairs and the structure becomes cubic. In the same way, when chromium percolates $PbTiO_3$, the second-order Jahn−Teller distortion that mixes the empty Ti 3d orbitals into the filled 2p orbitals of the oxygen is no longer possible and, again,[48] the B-site cations move to the center and the structure becomes cubic. In the $PbTi_{1-x}V_xO_3$ system there is no change in symmetry. However, after percolation, the d^1 electrons avoid the transition to a cubic phase with application of temperature. This also explains why an MPB is not observed in these systems.

In summary, $PbM_{1-x}M_x'O_3$ (M, M′ = Ti, Cr, and V) systems have been synthesized under high-pressure conditions. $PbTiO_3$ is percolated by vanadium and chromium, and after the percolation threshold, it starts to behave like the dopant. $PbVO_3$ is percolated by chromium and transforms to a cubic structure at the threshold. All three systems, after the percolation threshold, mimic the behavior of the cation with the most d electrons; thus, $PbTi_{1-x}V_xO_3$ follows vanadium's behavior, whereas $PbTi_{1-x}Cr_xO_3$ and $PbV_{1-x}Cr_xO_3$ follow that of chromium.

■ ASSOCIATED CONTENT

Ⓢ Supporting Information. Crystallographic data and supporting graphics. This material is available free of charge via the Internet at http://pubs.acs.org.

■ AUTHOR INFORMATION

Corresponding Author

*E-mail: aalopez@staffmail.ed.ac.uk.

Present Addresses

‡Centre for Science at Extreme Conditions, University of Edinburgh, Mayfield Road, EH9 3JZ Edinburgh, U.K.

■ ACKNOWLEDGMENT

We thank A. J. DosSantos-Garcia, J. Levin, and L. Clark for fruitful discussions and J. Gallardo-Amores, J. Romero de Paz, and E. Matesanz for technical assistance. Funding through projects MAT2007-64004 and Comunidad Autonoma de Madrid (MATERYENER program PRICYT S-0505/PPQ- 0093 and S-0505/PPQ0358) is acknowledged.

■ REFERENCES

(1) Arévalo-López, A. M.; Alario-Franco, M. *J. Solid State Chem.* **2007**, *180*, 3271.

(2) Burns, G.; Scott, B. A. *Phys. Rev. Lett.* **1970**, *25*, 167.

(3) Sanjurjo, J. A.; López-Cruz, E.; Burns, G. *Phys. Rev. B* **1983**, *28*, 7260.

(4) Pan, W. Y.; Dam, C. Q.; Zhang, Q. M.; Cross, L. E. *J. Appl. Phys.* **1989**, *66*, 6014.

(5) Heaney, P. J. In *Transformation Processes in Minerals*; Redfern, S. A., Carpenter, M. A., Eds.; Reviews in Mineralogy and Geochemistry; Mineralogical Society of America: Washington, DC, 2000; Vol. 39.

(6) Noheda, B. *Curr. Opin. Solid State Mater. Sci.* **2002**, *6*, 27.

(7) Grinberg, I.; Suchomel, M. R.; Davies, P. K.; Rappe, A. M. *J. Appl. Phys.* **2005**, *98*, 094111.

(8) G., S.; A., T. *J. Phys. Soc. Jpn.* **1952**, *7*, 5.

(9) Shirane, G.; Suzuki, K.; Takeda, A. *J. Phys. Soc. Jpn.* **1952**, *7*, 12.

(10) Shirane, G.; Suzuki, K. *J. Phys. Soc. Jpn.* **1952**, *7*, 333.

(11) Noheda, B.; Cox, D. E.; Shirane, G.; Park, S. E.; Cross, L. E.; Zhong, Z. *Phys. Rev. Lett.* **2001**, *86*, 3891.

(12) Ahart, M.; Somayazulu, M.; Cohen, R. E.; Ganesh, P.; Dera, P.; Mao, H.-K.; Hemley, R. J.; Ren, Y.; Liermann, P.; Wu, Z. *Nature* **2008**, *451*, 545.

(13) Shpanchenko, R. V.; Chernaya, V. V.; Tsirlin, A. A.; Chizhov, P. S.; Sklovsky, D. E.; Antipov, E. V.; Khlybov, E. P.; Pomjakushin, V.; Balagurov, A. M.; Medvedeva, J. E.; Kaul, E. E.; Geibel, C. *Chem. Mater.* **2004**, *16*, 3267–3273.

(14) Oka, K.; Yamada, I.; Azuma, M.; Takeshita, S.; Satoh, K.; Koda, A.; Kadono, R.; Takano, M.; Shimakawa, Y. *Inorg. Chem.* **2008**, *47*, 7355.

(15) Kumar, A.; Martin, L. W.; Denev, S.; Kortright, J. B.; Suzuki, Y.; Ramesh, R.; Gopalan, V. *Phys. Rev. B* **2007**, *75*, 060101.

(16) DeVries, R. C.; Roth, W. L. *J. Am. Ceram. Soc.* **1968**, *51*, 72.

(17) Roth, W. L.; DeVries, R. C. *J. Appl. Phys.* **1967**, *38*, 951.

(18) Chamberland, B. L.; Moeller, C. W. *J. Solid State Chem.* **1972**, *5*, 39.

(19) Arévalo-López, A. M.; DosSantos-García, A. J.; Alario-Franco, M. *Inorg. Chem.* **2009**, *48*, 5434.

(20) Rodriguez-Carvajal, J. FULLPROF: A program for Rietveld refinement and pattern matching analysis. *Abstract of the Satellite Meeting of the XVth Congress of the International Union of Crystallography*, Toulouse, France; Universite Paul Sabatier: Tolulouse, 1990; p127.

(21) Muller, D. A.; Singh, D.; Silcox, J. *Phys. Rev. B* **1998**, *57*, 8181.

(22) Egerton, R. F. *Electron Energy-Loss Spectroscopy in the Electron Microscope*; Plenum Press: New York, 1996.

(23) Ikemoto, I.; Ishii, K.; Kinoshita, S.; Kuroda, H.; Alario-Franco, M. A.; Thomas, J. M. *J. Solid State Chem.* **1976**, *17*, 425.

(24) Galindo, P.; Kret, S.; Sanchez, A. M.; Laval, J. Y.; Yañez, A.; Pizarro, J.; Guerrero, E.; Bem, T.; Molina, S. I. *Ultramicroscopy* **2007**, *107*, 1186.

(25) http://www2.uca.es/grup-invest/sic/straintool.htm.

(26) Shirane, G.; Hoshino, S.; Suzuki, K. *Phys. Rev.* **1950**, *80*, 1105.
(27) Ye, Z. G.; Noheda, B.; Dong, M.; Cox, D.; Shirane, G. *Phys. Rev. B* **2001**, *64*, 184114.
(28) Lebon, A.; Dammak, H.; Calvarin, G.; Ahmedou, I. O. *J. Phys.: Condens. Matter* **2002**, *14*, 7035.
(29) Noheda, B.; Cox, D. E.; Shirane, G.; Guo, R.; Jones, B.; Cross, L. E. *Phys. Rev. B* **2001**, *6301*, 014103.
(30) Yamada, Y.; Uesu, Y.; Matsuda, M.; Fujishiro, K.; Cox, D. E.; Noheda, B.; Shirane, G. *J. Phys. Soc. Jpn.* **2002**, *71*, 966.
(31) Noheda, B.; Cox, D. E.; Shirane, G.; Guo, R.; Jones, B.; Cross, L. E. *Phys. Rev. B* **2000**, *63*, 014103.
(32) Galy, J.; Meunier, G.; Andersson, S.; Astrom, A. *J. Solid State Chem.* **1975**, *13*, 142.
(33) Galy, J.; Enjalbert, R. *J. Solid State Chem.* **1982**, *44*, 1.
(34) Cohen, R. E. *Nature* **1992**, *358*, 136.
(35) Shannon, R. D. *Acta. Crystallogr., A* **1976**, *32*, 751.
(36) Khomskii, D. I. *J. Magn. Magn. Mater.* **2006**, *306*, 1.
(37) Waghmre, U. V.; Spaldin, N. A.; Kandpal, H. C.; Seshadri, R. *Phys. Rev. B* **2003**, *67*, 125111.
(38) Shirane, G.; Pepinsky, R.; Frazer, B. *Acta Crystallogr.* **1956**, *9*, 131.
(39) Oh, H. S.; Jang, H. M. *J. Appl. Phys.* **1999**, *85*, 2815.
(40) Belik, A. A.; Azuma, M.; Saito, T.; Shimakawa, Y.; Takano, M. *Chem. Mater.* **2005**, *17*, 269.
(41) Pearson, D.; Ahn, C.; Fultz, B. *Phys. Rev. B* **1993**, *47*, 8471.
(42) Shin, Y.-H.; Son, J.-Y.; Lee, B.-J.; Grinberg, I.; Rappe, A. M. *J. Phys.: Condens. Matter* **2008**, *20*, 015224.
(43) Tsirlin, A. A.; Belik, A.; Shpanchenko, R. V.; Antipov, E.; Takayama-Muromachi, E.; Rosner, H. *Phys. Rev. B* **2008**, *77*, 092402.
(44) Mentre, O.; Kanke, Y.; Dhaussy, A.-C.; Conflant, P.; Hata, Y.; Kita, E. *Phys. Rev. B* **2001**, *64*, 174404.
(45) Mentre, O.; Dhaussy, A.-C.; Abraham, F. *J. Solid State Chem.* **1997**, *130*, 223.
(46) Tarasevich, Y. Y.; Cherkasova, V. A. *Eur. Phys. J. B* **2007**, *60*, 97.
(47) Rivera, A.; Leon, C.; Santamaria, J.; Varez, A.; Vyunov, O.; Belous, A. G.; Alonso, J. A.; Sanz, J. *Chem. Mater.* **2002**, *14*, 5148.
(48) Kan, E.; Xiang, H.; Lee, C.; Wu, F.; Yang, J.; Whangbo, M.-H. *Angew. Chem., Int. Ed.* **2010**, *49*, 1603.